

Pressure-promoted ligand to metal energy transfer for emission enhancement of $[Tb_2(BDC)_3(DMF)_2(H_2O)_2]_n$ metal-organic framework

Yunfeng Yang(杨云峰), Kaiyan Yuan(袁开岩), Binhao Yang(杨斌豪), Qing Yang(杨青), Yixuan Wang(王艺璇), and Xinyi Yang(杨新一)

Citation: Chin. Phys. B, 2025, 34 (**3**): 036101. DOI: 10.1088/1674-1056/ada755
Journal homepage: http://cpb.iphy.ac.cn; http://iopscience.iop.org/cpb

What follows is a list of articles you may be interested in

Pressure-induced superconductivity and phase transition in PbSe and PbTe

Yuyang Jiang(江宇阳), Cuiying Pei(裴翠颖), Qi Wang(王琦), Juefei Wu(吴珏霏), Lili Zhang(张丽丽), Chao Xiong(熊超), and Yanpeng Qi(齐彦鹏)

Chin. Phys. B, 2024, 33 (**12**): 126105. DOI: 10.1088/1674-1056/ad8ecc

Pressure-induced structural transitions and metallization in $ZrSe_2$

Yiping Gao(高一平), Chenchen Liu(刘晨晨), Can Tian(田灿), Chengcheng Zhu(朱程程), Xiaoli Huang(黄晓丽), and Tian Cui(崔田)

Chin. Phys. B, 2024, 33 (**12**): 126104. DOI: 10.1088/1674-1056/ad8ec9

Pressure-induced structural, electronic, and superconducting phase transitions in $TaSe_3$

Yuhang Li(李宇航), Pei Zhou(周佩), Chi Ding(丁驰), Qing Lu(鲁清), Xiaomeng Wang(王晓梦), and Jian Sun(孙建)

Chin. Phys. B, 2024, 33 (**10**): 106102. DOI: 10.1088/1674-1056/ad6f92

First-principles study of structural and electronic properties of multiferroic oxide Mn_3TeO_6 under high pressure

Xiao-Long Pan(潘小龙), Hao Wang(王豪), Lei Liu(柳雷), Xiang-Rong Chen(陈向荣), and Hua-Yun Geng(耿华运)

Chin. Phys. B, 2024, 33 (**7**): 076102. DOI: 10.1088/1674-1056/ad3ef6

Ultrafast dynamics in photo-excited Mott insulator $Sr_3Ir_2O_7$ at high pressure

Xia Yin(尹霞), Jianbo Zhang(张建波), Wang Dong(王东), Takeshi Nakagawa, Chunsheng Xia(夏春生), Caoshun Zhang(张曹顺), Weicheng Guo(郭伟程), Jun Chang(昌峻), and Yang Ding(丁阳)

Chin. Phys. B, 2024, 33 (**1**): 016103. DOI: 10.1088/1674-1056/acdc8c

---

SPECIAL TOPIC — Structures and properties of materials under high pressure

Pressure-promoted ligand to metal energy transfer for emission enhancement of $[Tb_2(BDC)_3(DMF)_2(H_2O)_2]_n$ metal–organic framework

Yunfeng Yang(杨云峰), Kaiyan Yuan(袁开岩), Binhao Yang(杨斌豪), Qing Yang(杨青)[†], Yixuan Wang(王艺璇)[‡], and Xinyi Yang(杨新一)[§]

Synergetic Extreme Condition High-Pressure Science Center, State Key Laboratory of Superhard Materials, College of Physics, Jilin University, Changchun 130012, *China*

(Received 26 November 2024; revised manuscript received 4 January 2025; accepted manuscript online 8 January 2025)

Lanthanide metal–organic frameworks (Ln-MOFs) have received extensive attention in the development of photoluminescent (PL) materials due to their stable structures and unique line-like emission spectroscopic properties. However, in order to prepare Ln-MOFs with high PL quantum yield (PLQY), further improving the sensitization efficiency of the "antenna effect" is essential. Herein, remarkably enhanced PL in $[Tb_2(BDC)_3(DMF)_2(H_2O)_2]_n$ MOF is successfully achieved via high-pressure engineering at room temperature. Notably, the PL intensity continues to increase as the pressure increases, reaching its peak at 12.0 GPa, which is 4.4 times that of the initial state. Detailed experimental and theoretical calculations have demonstrated that pressure engineering significantly narrows the bandgap of $[Tb_2(BDC)_3(DMF)_2(H_2O)_2]_n$, optimizing both singlet and triplet energy levels. Ultimately, higher antenna effect sensitization efficiency is achieved by promoting intersystem crossing and energy transfer processes. Our work provides a promising strategy for the development of high PLQY Ln-MOFs.

Keywords: lanthanide metal–organic frameworks, high pressure, green light photoluminescence enhancement, energy transfer

PACS: 61.05.cp, 71.20.–b, 78.55.–m, 81.40.Vw

DOI: 10.1088/1674-1056/ada755 **CSTR:** 32038.14.CPB.ada755

1. Introduction

Trivalent lanthanide ions (Ln^{3+}) possess characteristic emission bands with narrow peak widths in the visible or near-infrared spectral regions, making them promising for applications in optical imaging, contactless sensing, and solid-state lighting.[1–3] However, the direct excitation of Ln^{3+} is very inefficient unless high-power laser excitation is utilized owing to the forbidden f–f transitions.[4] This problem can be overcome by utilizing organic linkers with strongly absorbing chromophores to sensitize Ln^{3+} emission, known as the "antenna effect".[5,6] The lanthanide metal–organic frameworks (Ln-MOFs) formed by the coordination of Ln^{3+} and organic chromophores have the dual advantage of protecting the metal ions from vibrational coupling and increasing the light-absorbing cross-section through the antenna effect.[7–9] The photoluminescence (PL) of Ln-MOFs is mainly achieved through the following two processes.[10] Firstly, upon excitation, the energy of the ligand transitions from the lowest singlet excited state (S_1) to the triplet excited state (T_n) through the intersystem crossing (ISC). Subsequently, the ultimate metal-centered PL is achieved by an energy transfer (ET) from the lowest triplet excited state energy level (T_1) of the ligand to the Ln^{3+} energy level. Therefore, improving the efficiency of the ISC and optimizing the energy alignment between the ligand's triplet state energy level and the Ln^{3+} energy level are essential for enhancing the PL quantum yield (PLQY) of Ln-MOFs.

Pressure serves as a potent strategy for regulating the crystal structure and electronic structure of materials without altering their chemical composition.[11–13] In recent years, a wide array of materials, including perovskites, semiconductor quantum dots, covalent organic frameworks, and MOFs, have exhibited pressure-induced emission enhancement (PIEE) and piezochromic behaviors.[14–17] Noteworthy, research has shown that pressure can facilitate the ISC process in isophthalic acid by boosting the mixing of n–π^*/π–π^* transition configurations in the triplet states.[18] Additionally, pressure can also effectively promote the ET process in Tb-MOFs by modulating the triplet energy levels of the ligands.[19] Therefore, it is entirely feasible to utilize pressure to enhance the sensitization efficiency of the antenna effect in Ln-MOFs. However, relevant research is still relatively scarce.

[†]Corresponding author. E-mail: yangqing21@mails.jlu.edu.cn
[‡]Corresponding author. E-mail: wangyixuan19@jlu.edu.cn
[§]Corresponding author. E-mail: yangxinyi@jlu.edu.cn

© 2025 Chinese Physical Society and IOP Publishing Ltd. All rights, including for text and data mining, AI training, and similar technologies, are reserved.

Herein, we selected $[Tb_2(BDC)_3(DMF)_2(H_2O)_2]_n$ MOFs as the research object to explore the evolution of its optical properties under high pressure. The high-pressure PL spectra and optical microscope images indicated that $[Tb_2(BDC)_3(DMF)_2(H_2O)_2]_n$ exhibits a significant PIEE behavior. Notably, the PL intensity was enhanced by 4.4 times at 12.0 GPa compared to the initial state. The high-pressure UV–visible absorption spectra, angle-dispersive x-ray diffraction (ADXRD), and theoretical calculations demonstrated that pressure can regulate the crystal structure and bandgap of $[Tb_2(BDC)_3(DMF)_2(H_2O)_2]_n$, thereby adjusting its singlet and triplet energy levels. The proximity of singlet and triplet energy levels of ligands improves the ISC efficiency. In addition, the proximity of the triplet energy level of the ligand and the energy level of Tb^{3+} promotes the ET process. Therefore, the high pressure enhances the transition dipole moment while optimizing the sensitization efficiency of the antenna effect, ultimately achieving the PL enhancement. This study provides a valuable approach to advancing the development of Ln-MOFs with high PLQY.

2. Experimental details

2.1. Sample preparation

A 3 ml aqueous solution of $Tb(NO_3)_2{\cdot}6H_2O$ (180 mg, 413 mmol) was mixed with 3 ml DMF solution of H_2BDC (benzene-1,4-dicarboxylic acid, 144 mg, 0.867 mmol) in a 25 ml weighing flask. The mixed solution was heated at 80 °C for 48 hours. The crystals were cooled and filtered, and then washed with DMF.[20]

2.2. High-pressure generation

The high pressure was generated by a symmetrical diamond anvil unit (DAC) device with an anvil size of 400 μm. Silicon oil (Aldrich) was utilized as the pressure transmitting medium (PTM) in the high-pressure measurements.

2.3. Characterization and measurements

The fiber optic spectrometers utilized for *in situ* UV–visible absorption spectroscopy measurements and *in situ* high-pressure PL spectroscopy measurements are both QE65000 ocean optics spectrometers. The excitation sources for UV–visible absorption and PL measurements are the deuterium–halogen light and the 365 nm line of the UV DPSS laser, respectively. With the use of a camera (Ecilipse TI-U, Nikon) mounted on a microscope (Canon Eos 5D Mark II), PL images of $[Tb_2(BDC)_3(DMF)_2(H_2O)_2]_n$ were captured.

In situ high-pressure ADXRD measurements were performed at the BL15U1 beamline in the Shanghai Synchrotron Radiation Facility (SSRF) and the 4W2 High Pressure Station in Beijing Synchrotron Radiation Facility (BSRF) with a wavelength of 0.6199 Å. We used CeO_2 as the standard sample to do the calibration. The Bragg diffraction rings were recorded by a Mar-345 CCD detector and integrated into a one-dimensional profile using the FIT2D program.

2.4. Methods of calculation

The first-principles density functional theory (DFT) calculations are performed using the plane-wave pseudopotential as implemented in the Vienna *ab-initial* simulation package (VASP) code.[21,22] The electron–core interactions are described with the frozen-core projector-augmented wave pseudopotentials as parameterization by the Perdew–Burke–Ernzerhof (PBE) as the exchange–correlation function with $4f^96s^2$ (Tb), $2s^22p^4$ (O), $2s^22p^3$ (N), $2s^22p^2$ (C), and $1s^1$ (H) treated explicitly as valence electrons.[23,24]

3. Result and discussion

3.1. Structure and PL stimuli-responsive behaviors of $[Tb_2(BDC)_3(DMF)_2(H_2O)_2]_n$

Scanning electron microscopy (SEM) image shows that the as-synthesized $[Tb_2(BDC)_3(DMF)_2(H_2O)_2]_n$ is a micron-sized crystal with a size of about 50 μm (Fig. S1). $[Tb_2(BDC)_3(DMF)_2(H_2O)_2]_n$ possesses a triclinic crystal structure (space group of *P*-1) with lattice parameters $a = 8.5716$ Å, $b = 10.1686$ Å, $c = 11.1262$ Å and $\alpha = 64.8764°$, $\gamma = 71.6924°$, $\beta = 79.1966°$ at ambient conditions. As shown in Fig. 1(a), seven of the oxygen atoms surrounding Tb^{3+} originate from four distinct carboxylic acid groups of BDC^{2-}, while the remaining two oxygen atoms stem from a water molecule and a DMF molecule, respectively.[19] Under the excitation of a 365 nm laser, $[Tb_2(BDC)_3(DMF)_2(H_2O)_2]_n$ emits the characteristic peaks of Tb^{3+} at 488 nm, 543 nm, 585 nm and 623 nm that are ascribed to $^5D_4 \rightarrow {}^7F_J$ ($J = 6$, 5, 4, and 3, respectively).[8] Among the transitions, the emission peak at 543 nm dominates, resulting in a strong green PL. The emission band of BDC^{2-} could not be observed in the short wavelength region, indicating the existence of highly efficient ET from BDC^{2-} to Tb^{3+}. We conducted *in situ* high-pressure PL experiments to investigate the optical properties of $[Tb_2(BDC)_3(DMF)_2(H_2O)_2]_n$ during compression from 1 atm to 16.6 GPa. As shown in Fig. 1(b), a gradual enhancement of the overall PL was observed with the pressure increased, reaching its maximum value at 12.0 GPa. The maximum PL intensity of the $^5D_4 \rightarrow {}^7F_5$ (543 nm) at 12.0 GPa is approximately 4.4 times that under ambient conditions. Compared with its initial value of 20.8%, $[Tb_2(BDC)_3(DMF)_2(H_2O)_2]_n$ exhibits a significant PLQY at 12.0 GPa, which was calculated to be 57.7% (Fig. S2 and Table S1). This is attributed to the fact that pressure effectively adjusts the energy levels of singlet and triplet states, promoting the ET process.[19] Upon higher

pressures, PL intensity begins to significantly decrease, and almost disappears at 16.6 GPa (Fig. 1(c)). To further explore the optical property evolution of $[Tb_2(BDC)_3(DMF)_2(H_2O)_2]_n$, we collected *in situ* high-pressure PL micrographs during compression (Fig. 1(d)). The optical micrographs clearly reveal the trend from dark green to bright green of PL intensity during the compression.

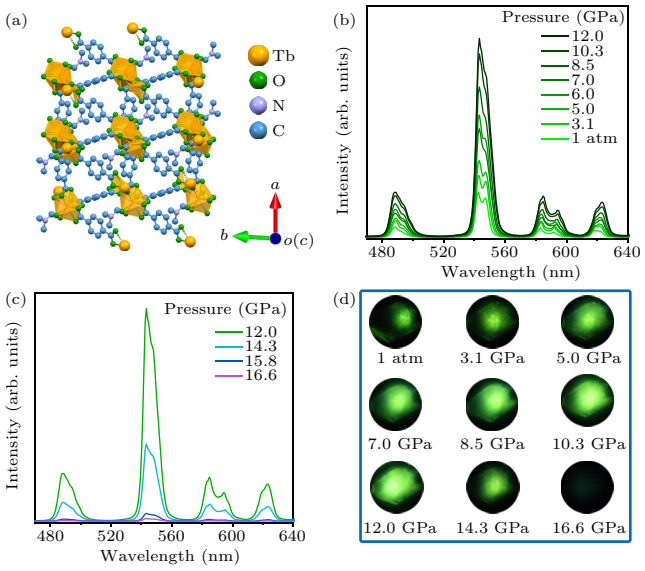


Fig. 1. The structure and PL stimuli-responsive behaviors of $[Tb_2(BDC)_3(DMF)_2(H_2O)_2]_n$. (a) Crystallographic view along the *c*-axis (H atoms were omitted for clarity). [(b) and (c)] PL spectra as a function of pressure. (d) Optical images under different pressures.

3.2. The evolution of absorption and bandgap of $[Tb_2(BDC)_3(DMF)_2(H_2O)_2]_n$ under pressure

To elucidate the origin of the significant PIEE behavior observed in the $[Tb_2(BDC)_3(DMF)_2(H_2O)_2]_n$, we recorded their pressure-dependent UV–visible absorption spectra (Fig. 2(a)). At ambient conditions, a steep absorption edge is observed at about 310 nm. With increasing pressure, the absorption edge experiences a persistent redshift. When the pressure exceeds 12.0 GPa, the absorption edge exhibits a sharper redshift, indicating that the emergence of structural transformation affects the distribution of electronic states.[25,26] The extraordinary piezochromic transition of the $[Tb_2(BDC)_3(DMF)_2(H_2O)_2]_n$ is evidently seen through optical micrographs in a symmetric DAC apparatus (Fig. 2(b)). After compression, the originally transparent colorless crystal transforms into a pale-yellow crystal, corresponding to absorption spectra changes.[27] The evolution of optical bandgap can be effectively evaluated based on the motion of the absorption edge. The bandgaps are estimated from the Tauc plot by plotting $(\alpha h\nu)^2$ versus $h\nu$ to determine the intercept with the energy axis, where α is the absorption coefficient and $h\nu$ is the photon energy. As shown in Fig. 2(c), $[Tb_2(BDC)_3(DMF)_2(H_2O)_2]_n$ exhibits an indirect gap of 3.91 eV at ambient conditions. As the pressure increases, the bandgap of $[Tb_2(BDC)_3(DMF)_2(H_2O)_2]_n$ undergoes a continuously noticeable reduction process. During the compression from 1 atm to 12.0 GPa, the bandgap significantly narrows from 3.91 eV to 3.32 eV (Fig. 2(d)). Below 12.0 GPa, the bandgap decreases at a rate of −53.04 meV/GPa, slower than that at higher pressures (−132.12 meV/GPa), indicating an electronic structure transition. The transformation of electronic structure results in no further enhancement of PL intensity under high pressure.

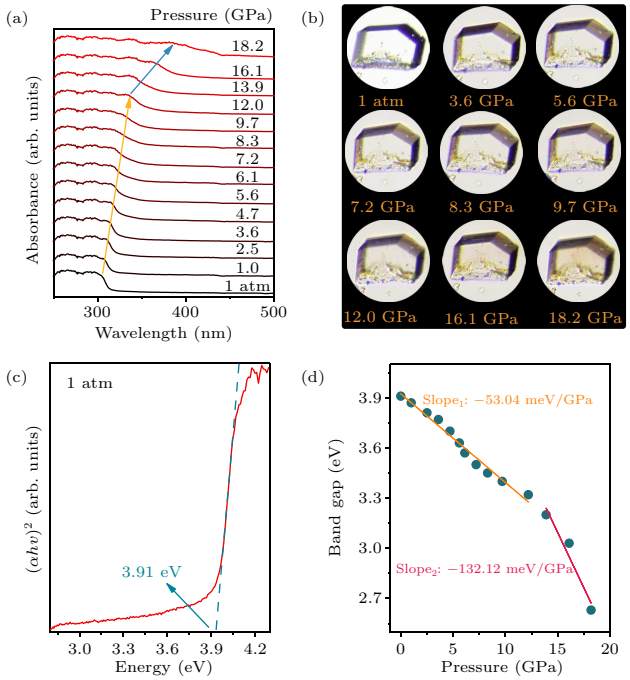


Fig. 2. The evolution of absorption and bandgap with pressure of $[Tb_2(BDC)_3(DMF)_2(H_2O)_2]_n$. (a) Optical absorption spectra under high pressure. (b) Optical micrograph in a DAC during compression. (c) The Tauc plot at ambient conditions. (d) Bandgap evolutions under high pressure.

3.3. Structural evolution of $[Tb_2(BDC)_3(DMF)_2(H_2O)_2]_n$ under pressure

In situ high-pressure ADXRD experiments were further performed to explore the relationship between the structure and the optical properties of $[Tb_2(BDC)_3(DMF)_2(H_2O)_2]_n$ (Fig. 3(a)). With increasing pressure, almost all Bragg diffraction peaks are shifted to the larger 2θ range before 12.0 GPa. However, due to the different movement rates of each crystal plane during the compression process, some diffraction peaks may merge or split. It is noteworthy that the (011) plane located at 4.1° consistently shifts towards lower 2θ with pressure increasing. This is due to the fact that the (011) plane is perpendicular to the long diagonal of the "wine rack" configuration, which is prone to negative compression under high pressure (Fig. S3).[16,28] Upon further compression, it is observed that all diffraction peaks disappear, indicating the generation of structural distortion and the appearance of an amorphous state.[11,12] Rietveld refinements are performed on the ADXRD spectra by General Structure Analysis System

(GSAS) software to gain detailed information about the structural evolution of $[Tb_2(BDC)_3(DMF)_2(H_2O)_2]_n$ under high pressure. The refinement of the XRD patterns matches well with the calculated data (Figs. 3(b) and S4). The refinement results show that all particles before 12.0 GPa belong to the *P*-1 space group, indicating that the symmetry did not change during the compression process. The pressure volume data is fitted by the third-order Birch–Murnaghan equation of state, as follows:[14]

$$P(V) = \frac{3B_0}{2}\left[\left(\frac{V_0}{V}\right)^{\frac{7}{3}} - \left(\frac{V_0}{V}\right)^{\frac{5}{3}}\right] \times \left\{1 + \frac{3}{4}(B' - 4)\left[\left(\frac{V_0}{V}\right)^{\frac{2}{3}} - 1\right]\right\}.$$

Here V_0 is the zero-pressure volume, B_0 is the bulk modulus at ambient pressure, and B' is a parameter for pressure derivative. Continuous volume collapse before 12.0 GPa suggests no phase transition has occurred (Fig. 3(c)). All lattice constants remain continuous throughout the entire compression process (Fig. S5). However, the unit cells of the sample exhibit anisotropic compression under pressure, which may account for the amorphization after 12.0 GPa. As shown in Fig. 3(d), Tb^{3+} coordinates with three BDC molecules in different coordinations. The distances between Tb^{3+} and the carboxyl carbon atoms of the three BDC^{2-} molecules are d_I, d_{II} and d_{III}. With the pressure increasing, the distance between Tb^{3+} and the three BDC^{2-} molecules gradually decreases, which enhances the heavy atom effect and leads to emission enhancement (Fig. 3(e)).[29] The heavy atom effect enhances spin–orbit coupling, thereby promoting the intersystem crossing process from S_1 to T_n.[30,31]

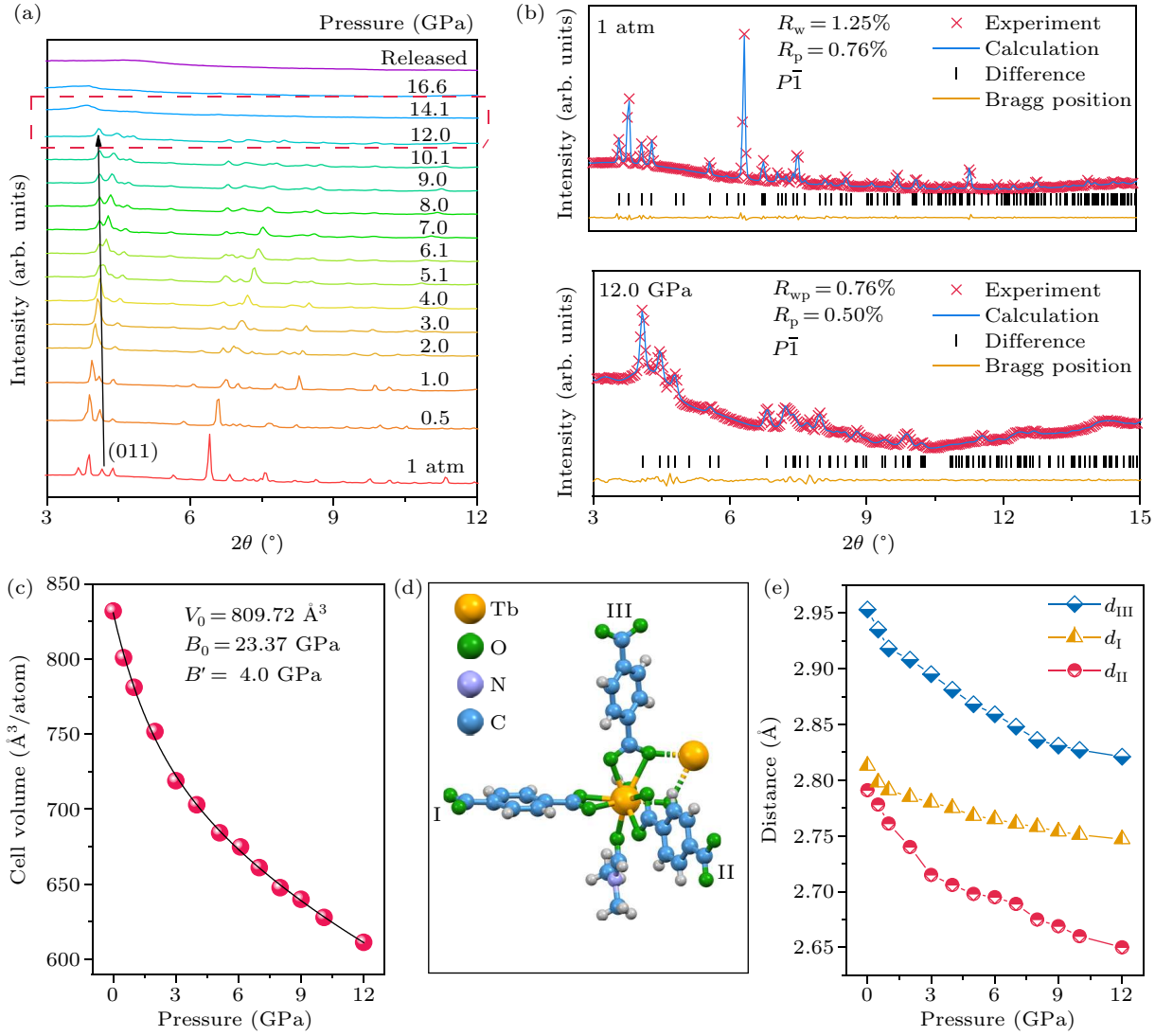


Fig. 3. Structural evolution of $[Tb_2(BDC)_3(DMF)_2(H_2O)_2]_n$ under pressure. (a) *In situ* high-pressure ADXRD patterns of $[Tb_2(BDC)_3(DMF)_2(H_2O)_2]_n$ under different pressures. (b) Rietveld refinements of ADXRD patterns collected at 1 atm and 12.0 GPa. (c) Changes in the unit cell volume of $[Tb_2(BDC)_3(DMF)_2(H_2O)_2]_n$ during compression. (d) Local structural diagram of $[Tb_2(BDC)_3(DMF)_2(H_2O)_2]_n$. (e) The distances between Tb^{3+} and the carboxyl carbon atoms of the three BDC^{2-} molecules.

3.4. Theoretical calculation

In addition, to clearly explore the mechanism of PL enhancement, we examined the electronic properties for the periodic structure of $[Tb_2(BDC)_3(DMF)_2(H_2O)_2]_n$ by DFT calculations. The calculation results show that the bandgap energy at ambient conditions is 3.30 eV, which is significantly lower than the experimental measurement result of 3.91 eV (Fig. 4(a)). The reason for this result is that the Perdew–Burke–Ernzerhof (PBE) functional contains unphysical self-Coulomb repulsion, leading to a systematic underestimate of bandgaps.[24,32] It is worth noting that the theoretical bandgap energy of $[Tb_2(BDC)_3(DMF)_2(H_2O)_2]_n$ at 12.0 GPa is decreased by 0.52 eV compared to that at ambient conditions, which is consistent with experimental results (Fig. 4(b)). In addition, the dipole transition matrix components (P^2) at ambient conditions and high pressure are calculated to reveal the high transition probabilities between the topmost valence band and the lowest conduction band.[33] The P^2 at various high-symmetry k points increases significantly under high pressure, reflecting the observed enhancement of PL.[34] To sum up, the bandgap reduction indicates a decrease in the S_1 and T_n energy levels of the ligand, resulting in a smaller energy difference (ΔE_{S-T}) and facilitating the ISC process (Fig. 4(c)).[18] Meanwhile, the heavy atom effect caused by the shortened distance between Tb^{3+} and the ligand under high pressure further promotes the ISC process.[27] In addition, the proximity of the triplet energy level of the ligand and the energy level of Tb^{3+} (ΔE_{T-D}) promotes the ET process.[19] With the above considerations, high-pressure optimizes the sensitization efficiency of the "antenna effect" and increases the transition dipole moment, ultimately leading to the enhanced PL emission. Further compression results in amorphization of $[Tb_2(BDC)_3(DMF)_2(H_2O)_2]_n$. Symmetry breaking alters the original electronic configuration, leading to a gradual weakening of the PL.

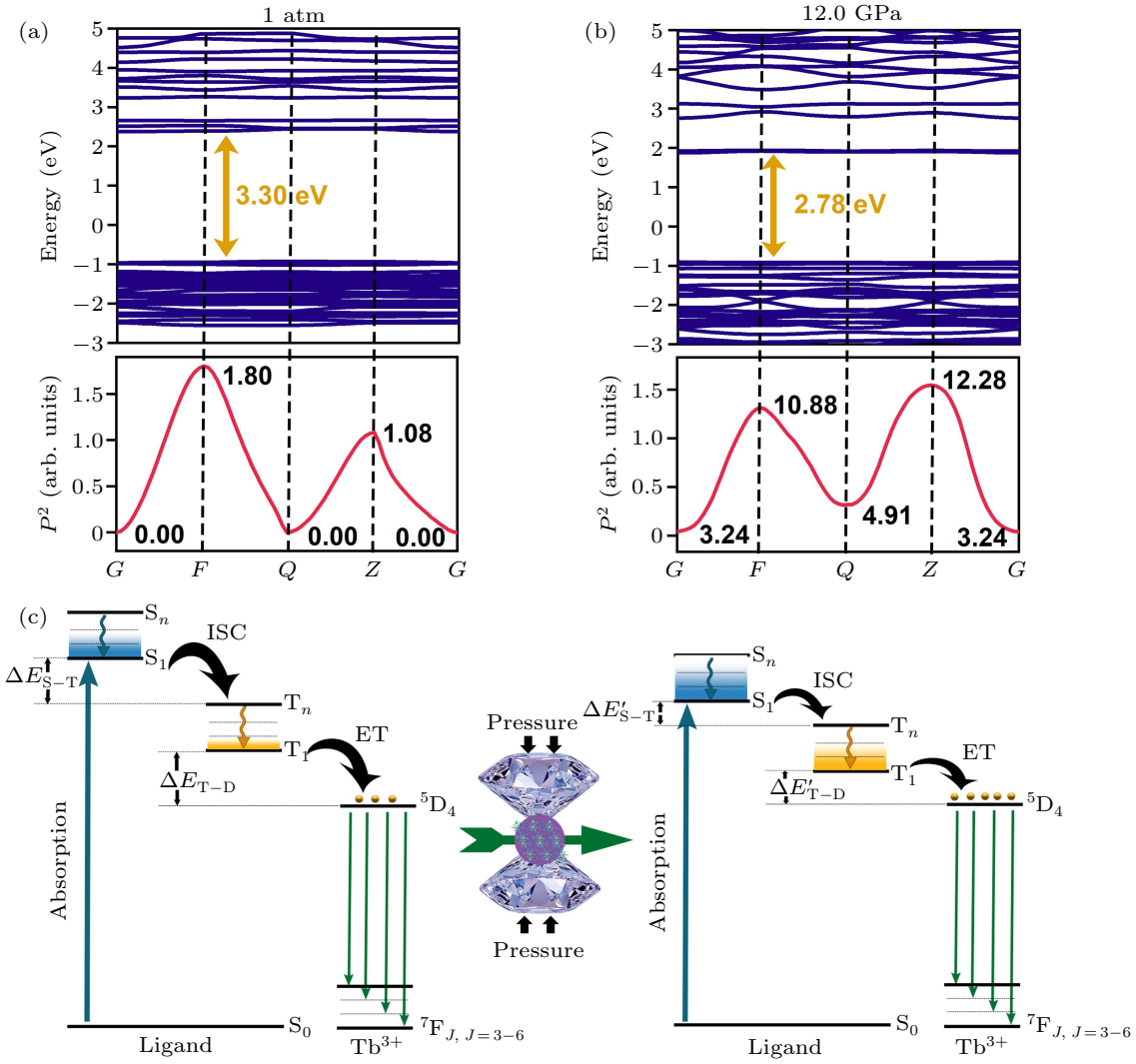


Fig. 4. PL mechanism of $[Tb_2(BDC)_3(DMF)_2(H_2O)_2]_n$. (a) and (b) PBE calculated band structures and transition matrix elements for $[Tb_2(BDC)_3(DMF)_2(H_2O)_2]_n$ at 1 atm and 12.0 GPa. (c) The schematic diagram of PL mechanism for $[Tb_2(BDC)_3(DMF)_2(H_2O)_2]_n$ at 1 atm and high pressure.

4. Conclusion

In summary, we studied the optical and structural pressure response of $[Tb_2(BDC)_3(DMF)_2(H_2O)_2]_n$ by high-pressure technology. $[Tb_2(BDC)_3(DMF)_2(H_2O)_2]_n$ exhibits PIEE behavior under high pressure. The PL intensity increases significantly with increasing pressure, reaching a maximum at 12.0 GPa, which is 4.4 times that of the initial state. Comprehensive analysis of experimental and DFT calculation results show that the high-pressure reduces the bandgap energy of $[Tb_2(BDC)_3(DMF)_2(H_2O)_2]_n$, resulting in a significant decrease in the energy levels of the singlet states and triplet states of the ligand. The proximity of ligand singlet and triplet energy levels optimizes the ISC process, while the proximity of the triplet energy level of the ligand and the energy level of Tb^{3+} promotes the ET process. Thus, high-pressure optimizes the sensitization efficiency of the "antenna effect" while improving the transition dipole moment, resulting in PL enhancement. This study offers a promising strategy for facilitating the development of high PLQY Ln-MOFs.

Acknowledgments

Project supported by the National Natural Science Foundation of China (Grant Nos. 12304261 and 12274177) and the China Postdoctoral Science Foundation (Grant No. 2024M751076). Angle dispersive XRD measurements were performed at the BL15U1 beamline in Shanghai Synchrotron Radiation Facility (SSRF) and the 4W2 High Pressure Station in Beijing Synchrotron Radiation Facility (BSRF).

References

[1] Bünzli J C G 2006 *Acc. Chem. Res.* **39** 53
[2] Heffern M C, Matosziuk L M and Meade T J 2014 *Chem. Rev.* **114** 4496
[3] Zhou J, Liu Q, Feng W, Sun Y and Li F 2015 *Chem. Rev.* **115** 395
[4] Vicinelli V, Ceroni P, Maestri M, Balzani V, Gorka M and Vögtle F 2002 *J. Am. Chem. Soc.* **124** 6461
[5] Bekiari V and Lianos P 1998 *Adv. Mater.* **10** 1455
[6] Weissman S I 1942 *J. Chem. Phys.* **10** 214
[7] Feng J and Zhang H 2013 *Chem. Soc. Rev.* **42** 387
[8] Lustig W P, Wang F, Teat S J, Hu Z, Gong Q and Li J 2016 *Inorg. Chem.* **55** 7250
[9] Liu Q, Yu J and Hu J 2024 *Chin. Phys. B* **33** 017204
[10] Cui Y, Xu H, Yue Y, Guo Z, Yu J, Chen Z, Gao J, Yang Y, Qian G and Chen B 2012 *J. Am. Chem. Soc.* **134** 3979
[11] Wang Z, Schliehe C, Wang T, Nagaoka Y, Cao Y C, Bassett W A, Wu H, Fan H and Weller H 2011 *J. Am. Chem. Soc.* **133** 14484
[12] Wang T, Li R, Quan Z, Loc W S, Bassett W A, Xu H, Cao Y C, Fang J and Wang Z 2015 *Adv. Mater.* **27** 4544
[13] Guo S, Li Y, Mao Y, Tao W, Bu K, Fu T, Zhao C, Luo H, Hu Q, Zhu H, Shi E, Yang W, Dou L and Lü X 2022 *Sci. Adv.* **8** eadd1984
[14] Ma Z, Liu Z, Lu S, Wang L, Feng X, Yang D, Wang K, Xiao G, Zhang L, Redfern S A T and Zou B 2018 *Nat. Commun.* **9** 4506
[15] Wu M, Liu H, Liu H, Lu T, Wang S, Niu G, Sui L, Bai F, Yang B, Wang K, Yang X and Zou B 2022 *J. Phys. Chem. Lett.* **13** 2493
[16] Yang Y, Wang Y, Bai F Q, Li S X, Yang Q, Wang W, Yang X and Zou B 2024 *Nano Lett.* **24** 9898
[17] Wang Y, Yang Y, Yang X and Zou B 2024 *Sci. China Chem.* **67** 2890
[18] Yang Q, Yang X, Wang Y, Fei Y, Li F, Zheng H, Li K, Han Y, Hattori T, Zhu P, Zhao S, Fang L, Hou X, Liu Z, Yang B and Zou B 2024 *Nat. Commun.* **15** 7778
[19] Wang Y, Yang X, Liu C, Liu Z, Fang Q, Bai F, Wang S, Hou X, Feng B, Chen B and Zou B 2022 *Angew. Chem. Int. Ed.* **134** e202210836
[20] Panyarat K, Ngamjarurojana A and Rujiwatra A 2019 *J. Photoch. Photobio. A* **377** 167
[21] Kresse G and Furthmüller J 1996 *Comp. Mater. Sci.* **6** 15
[22] Kresse G and Furthmüller J 1996 *Phys. Rev. B* **54** 11169
[23] Blöchl P E 1994 *Phys. Rev. B* **50** 17953
[24] Perdew J P, Burke K and Ernzerhof M 1996 *Phys. Rev. Lett.* **77** 3865
[25] Wang Y, Lü X, Yang W, Wen T, Yang L, Ren X, Wang L, Lin Z and Zhao Y 2015 *J. Am. Chem. Soc.* **137** 11144
[26] Jaffe A, Lin Y, Beavers C M, Voss J, Mao W L and Karunadasa H I 2016 *ACS Cent. Sci.* **2** 201
[27] Zhang L, Liu C, Wang L, Liu C, Wang K and Zou B 2018 *Angew. Chem. Int. Ed.* **57** 11213
[28] Li W, Probert M R, Kosa M, Bennett T D, Thirumurugan A, Burwood R P, Parinello M, Howard J A K and Cheetham A K 2012 *J. Am. Chem. Soc.* **134** 11940
[29] Zhao F, Hu J, Guan D, Liu J, Zhang X, Ling H, Zhang Y and Liu Q 2023 *Adv. Mater.* **35** 2304907
[30] Zhang P, Ke J, Tu D, Li J, Pei Y, Wang L, Shang X, Guan T, Lu S, Chen Z and Chen X 2022 *Angew. Chem. Int. Ed.* **61** e202112125
[31] Zhou B, Qi Z and Yan D 2022 *Angew. Chem. Int. Ed.* **61** e202208735
[32] Crowley J M, Tahir-Kheli J and Goddard W A 2016 *J. Phys. Chem. Lett.* **7** 1198
[33] Meng W, Wang X, Xiao Z, Wang J, Mitzi D B and Yan Y 2017 *J. Phys. Chem. Lett.* **8** 2999
[34] Luo J, Wang X, Li S, Liu J, Guo Y, Niu G, Yao L, Fu Y, Gao L, Dong Q, Zhao C, Leng M, Ma F, Liang W, Wang L, Jin S, Han J, Zhang L, Etheridge J, Wang J, Yan Y, Sargent E H and Tang J 2018 *Nature* **563** 541